

# Contribution of high- $nl$ shells to electron-impact ionization process

V. Jonauskas,<sup>1,\*</sup> A. Kynienė,<sup>1</sup> G. Merkelis,<sup>1</sup> G. Gaigalas,<sup>1</sup> R. Kisielius,<sup>1</sup> S. Kučas,<sup>1</sup> Š. Masys,<sup>1</sup> L. Radžiūtė,<sup>1</sup> and P. Rynkun<sup>1</sup>

<sup>1</sup>*Institute of Theoretical Physics and Astronomy,  
Vilnius University, A. Goštauto 12, LT-01108 Vilnius, Lithuania*

## Abstract

Contribution to electron-impact ionization cross sections from excitations to high- $nl$  shells and a consequent autoionization is investigated. We perform relativistic subconfiguration-average and detailed level-to-level calculations for this process. Ionization cross sections for the  $W^{27+}$  ion are presented to illustrate large influence of the high shells ( $n \geq 9$ ) and orbitals ( $l \geq 4$ ) in the excitation-autoionization process. The obtained results show that the excitations to the high shells ( $n \geq 9$ ) increase cross sections of indirect ionization process by a factor of two compared to the excitations to the lower shells ( $n \leq 8$ ). The excitations to the shells with the orbital quantum number  $l = 4$  give the largest contribution compared with the other orbital quantum numbers  $l$ . Radiative damping reduces the cross sections of the indirect process approximately two times in the case of the level-to-level calculations. Determined data show that the excitation-autoionization process contributes approximately 40% to the total ionization cross sections.

---

\* Valdas.Jonauskas@tfai.vu.lt

## I. INTRODUCTION

Energy losses from heavy elements, such as tungsten, due to radiative emission are one of the crucial problems to be overcome for the successful performance of the mononuclear reactors. Nevertheless, tungsten is used as the plasma-facing component in the modern fusion facilities because of its essential properties, like high-energy threshold for sputtering, low sputtering yield, and excellent thermal features. Even small concentration of tungsten ions ( $\sim 10^{-4}$ ) relative to the electron density prevents ignition of a deuterium-tritium plasma [1]. Theoretical modeling provides information about processes in such harsh conditions. However, fusion plasma modeling requires a significant amount of atomic data. The ionization and recombination processes determine the charge-state distribution in plasma. The electron-impact single ionization is the strongest one among the ionization processes. Contribution of the double ionization as a rule is much weaker compared with the single ionization. Furthermore, study of the double ionization process is quite complicated [2–4].

Electron-impact ionization for singly charged tungsten ions was previously studied by using the crossed-beam technique [5]. These data were supplemented by the electron-impact single, double, and triple ionization measurements of  $W^{q+}$  ions in the charge states  $q = 1 - 10$ ,  $q = 1 - 6$ , and  $q = 1 - 4$ , respectively [6, 7]. The configuration-average distorted-wave (CADW) calculations provided good agreement with experimental measurements for higher ionization stages ( $q \geq 4$ ) [8]. The DW approach succeeded in getting a very good agreement with experiment for the ionization stages up to  $W^{9+}$  ion and therefore it was applied to all isonuclear sequence [9]. Further level-to-level studies [10] included W atom and  $W^{2+}$  ion in the binary-encounter-dipole model as well as  $W^{4+}$  and  $W^{6+}$  ions in the DW approach. For the tungsten isonuclear sequence, cross sections were calculated using semirelativistic and relativistic DW methods for configurations and subconfigurations, respectively

[9]. Influence of the excitation-autoionization (EA) process, radiative damping, and relativistic effects were analyzed. The work of Loch et al. [9] considered the electron-impact excitations to all shells with  $n \leq 8$  and  $l \leq 3$ . The investigation has determined that the EA contribution is relatively small compared to direct ionization (DI) for the  $W^{11+}$  to  $W^{27+}$  ions. However, later experimental measurements for the  $W^{17+}$  ion have demonstrated a significant role of indirect process [11]. Theoretical study of cross sections using the Dirac-Fock-Slater approach confirmed these findings [12]. Furthermore, the authors found that Maxwellian rate coefficients are larger than the CADW rate coefficients by about 16%. The discrepancy was attributed to the EA channels originating from the high- $n$  shells up to  $n = 38$ .

Therefore, the main aim of our work is to determine the influence of excitations to the high- $n$  shells which lead to the EA process. For the study, we have chosen the  $W^{27+}$  ion which has only one  $4f$  electron in the valence shell. At first, we will present calculated results of the EA contribution for subconfigurations. Later, level-to-level distorted-wave (LLDW) data in a single configuration approach are analyzed. In addition, the influence of the radiative damping is studied in both cases. The contribution of the direct and indirect processes is compared for the  $W^{27+}$  ion.

## II. THEORETICAL APPROACH

Direct and indirect processes contribute to the total electron-impact single-ionization cross sections from the level  $i$  of  $A^{q+}$  ion to the level  $j$  of  $A^{(q+1)+}$  ion:

$$\sigma_{ij}(\varepsilon) = \sigma_{ij}^{\text{DI}}(\varepsilon) + \sum_k \sigma_{ik}^{\text{exc}}(\varepsilon) B_{kj}, \quad (1)$$

where  $\sigma_{ij}^{\text{DI}}(\varepsilon)$  is the direct ionization cross section at the electron energy  $\varepsilon$ ,  $\sigma_{ik}^{\text{exc}}$  is the electron-impact excitation cross section to the level  $k$  of the  $A^{q+}$  ion. Autoionization

branching ratio  $B_{kj}$  is determined by the expression:

$$B_{kj} = \frac{A_{kj}^a + \sum_n A_{kn}^r B_{nj}}{\sum_m A_{km}^a + \sum_n A_{kn}^r}, \quad (2)$$

where  $A^a$  and  $A^r$  are the Auger and radiative transition probabilities, respectively. Therefore, inclusion of the branching ratios in the cross section calculations leads to the radiative damping of the indirect process. The second term in the numerator presents the transition from the level  $k$  of the initial ion to the level  $j$  of the final ion through the intermediate levels  $n$  of the initial ion reached by the radiative transitions. This term is not studied in the current work because the amount of calculations drastically increases. Thus, the indirect ionization consists of the two-step process: the excitation with subsequent autoionization. It is evident that the branching ratios for the levels below the ionization threshold are equal to zero. Furthermore, the branching ratios are equal to zero for the levels above the ionization threshold if they cannot decay through the Auger transitions directly or through the intermediate states. The total ionization cross section for the initial level  $i$  is obtained by performing summation over the all final levels  $j$  in Eq. (1).

We do not consider higher order indirect ionization process such as a resonant-excitation double-autoionization. Previous analysis of this process for the  $W^{17+}$  ion determined a negligible contribution for the ionization cross sections [12].

The electron-impact excitation and ionization cross sections are determined in the DW approximation using the Flexible Atomic Code (FAC) [13] which implements the Dirac-Fock-Slater method. For moderate and highly charged ions, the direct ionization is accurately described by the DW approximation. The ionization cross sections are calculated in the potential of the ionizing ion. Calculations in the potential of the ionized ion provide approximately 10% smaller cross sections for the direct ionization.

### III. RESULTS

The ground configuration of the  $W^{27+}$  ion is  $[Kr]4d^{10}4f$  which consists of two levels. Our analysis of the ionization cross sections is based on the study of the ground level ( $4f_{5/2}$ ). Cross sections from the first excited level ( $4f_{7/2}$ ) are similar to the ones from the ground level and are not presented here.

The lowest two configurations of the  $W^{27+}$  ion together with the configurations which energy levels straddle the ionization threshold are shown in Fig. 1. The presented configurations with the energy levels near the ionization threshold are produced by the one-electron promotions from the ground configuration of the  $W^{27+}$  ion. They mainly correspond to the excitations from the  $4d$  shell up to the shells with  $n \leq 8$ . All of these configurations, except for the  $4d^9 4f 8d$  one, have average energies below the ionization threshold. Thus, they do not provide contribution to the ionization cross sections in the CADW approach. A few configurations formed by promotion from the  $4p$  shell also straddle the ionization threshold. However, the one-electron excitations reach only  $n = 6$  shell in this case.

The ionization process affecting the  $4s$ ,  $4p$ ,  $4d$ , and  $4f$  shells contribute to the DI process. On the other hand, study of the  $W^{17+}$  ion has demonstrated that ionization from the  $4s$  shell lies above the double-ionization threshold and contributes to the indirect double-ionization process [12].

Table I shows calculated energy levels for the lowest configurations of the  $W^{27+}$ ,  $W^{28+}$ , and  $W^{29+}$  ions. In addition, the lowest levels of the configurations for the  $W^{28+}$  ion produced from the ground configuration of the  $W^{27+}$  ion after an electron is ionized from the  $3d$ ,  $4s$ ,  $4p$ , or  $4d$  shells are shown. One can see that the calculated ionization threshold energy equals to 878.89 eV. The ionization energy obtained from the scaled electron binding energies is given as  $881.40 \pm 1.61$  eV [14]. That is in quite close agreement with our determined value. The ionization of the long-

living level of the  $[\text{Kr}]4d^{10}5s$  configuration corresponds to threshold energy 739.56 eV. This configuration can decay to the ground configuration through the weak electric octupole transitions (lifetime  $2.16 \cdot 10^2$  s).

Figure 2 shows contribution of the EA channels originating from the excitations to the high- $n$  shells up to  $n = 40$ . These data have been produced using the subconfiguration-average distorted-wave (SCADW) approach. As it was mentioned earlier, the previous study using the semirelativistic CADW calculations included only the excitations to the outer shells with  $n \leq 8$  and  $l \leq 3$  [9]. It can be seen from Fig. 2 that the additional EA channels originating from the excitations to the higher shells increase cross sections for the indirect part approximately by factor of two. The convergence for the cross sections is reached when the excitations to the high- $n$  shells are included. Furthermore, our calculations take into account the excitations to the shells with  $l \leq 6$ . Fig. 3 shows that the largest contribution to the EA process comes from the inner shell excitations to the  $l = 4$  orbital. The same trend is observed for the  $n \leq 8$  and  $9 \leq n \leq 25$  shells. However, the contribution to the EA process of the excitations to the  $l = 4$  orbital decreases if compared with other orbitals in the latter case. It is interesting that none of the excitations from the  $4s$ ,  $4p$ , or  $4d$  shells to the  $l = 4$  orbital give the largest cross sections. However, the total contribution of the excitations from the  $4s$ ,  $4p$ , and  $4d$  shells to the  $l = 4$  orbital is the largest compared to other orbitals. It is worth to note that excitations to  $l = 5$  orbital lead to the strong EA channel for which the relative contribution increases for  $9 \leq n \leq 25$  shells (Fig. 3b). For these shells, the largest increase of the relative contribution occurs for the excitations to a  $l = 2$  orbital compared to the  $n \leq 8$  case. This can be explained by the fact that the strongest excitations to the  $l = 2$  orbital take place from the  $4d$  shell. However, the configurations  $4d^9 4f n d$  with  $n = 5, 6, 7$  are below the ionization threshold, and they do not contribute to the EA process. Only some levels of the  $4d^9 4f 8d$  configuration are above the ionization

threshold (Fig. 1). On the other hand, all levels of  $4d^9 4f 8g$  configuration are above the ionization threshold. Furthermore, the energy levels of the  $4d^9 4f 7g$  configuration straddle the ionization threshold. It explains much larger relative contribution to the EA process of the excitations to the  $l = 4$  orbital for  $n \leq 8$  shells.

Other interesting result occurs when the EA channel originating from excitations to the  $l = 3$  orbital starts to dominate at high electron energies for the  $9 \leq n \leq 25$  shells. Contribution of the EA channel to the  $l = 4$  orbital is slightly smaller at the higher energies when the excitations to the large principal quantum numbers  $n$  are considered (Fig. 3b).

The EA channel for the excitations from the  $4d$  shell is predicted to produce the largest contribution compared to the EA channels from the  $4s$  and  $4p$  shells because the excitation cross sections are larger for the  $4d$  shell. However, as it is mentioned above, many configurations produced by the promotion from the  $4d$  shell to the  $nl$  shell for  $n \leq 8$  are below the ionization threshold. Therefore, these configurations do not contribute to the EA process. Figure 4a demonstrates that the contribution of the excitations from the  $4d$  shell to the EA process for  $n \leq 8$  is more than two times smaller compared to the EA channel for the excitations from the  $4p$  shell. The similar result was obtained for the  $W^{17+}$  ion when the excitations only up to  $n \leq 8$  were considered [12]. However, the situation drastically changes for the excitations from the  $4d$  to the higher shells because all arising configurations are above the ionization threshold (Fig. 4b). Contribution of this EA channel is much larger compared to the EA channel from the  $4p$  shell. Furthermore, the contribution of the EA channel from the  $4d$  shell for the excitations to  $9 \leq n \leq 25$  shells is comparable to the total cross sections of the EA process for the excitations to  $n \leq 8$  shells (Fig. 4a).

Calculations of the EA process for subconfigurations can differ from those for the detailed level-to-level studies. In our SCADW calculations, the energy levels are grouped into the subconfigurations. For the energy levels that straddle the ionization

threshold, the corresponding energy of the subconfiguration can be above or below the ionization threshold. The subconfiguration with the energy above the ionization threshold contributes to the EA process. Therefore, all levels of the subconfiguration, even those located below the ionization threshold, are included when the cross sections are calculated. On the other hand, for the subconfiguration below the ionization threshold, the contributions from the corresponding energy levels above the ionization threshold are neglected.

It is interesting to note that the EA cross sections obtained using SCADW and LLDW approaches are in good agreement when the autoionization branching ratios are not included in calculations (Fig. 5). Figure 5 shows that the radiative damping has the large impact on the ionization cross sections. However, it was found in the previous study that the autoionization branching ratios are close to 1 for this ionization stage [9]. The difference can be explained by the fact that the previous study used the configuration-average quantities while the current SCADW calculations employ the subconfigurations. The higher values of the cross sections for the SCADW calculations compared to the LLDW results suggest that the autoionization branching ratios for the CADW data are closer to 1. Therefore, the radiative decay paths are restricted for some excited configurations in these two averaged approaches. Figure 5 demonstrates that the level-to-level study is crucial for the EA process in the  $W^{27+}$  ion.

Figure 6 presents the total ionization cross sections for the direct and indirect ionization parts where the indirect part accounts for the radiative damping. In this case, the level-to-level calculations are presented. The contributions of DI from the  $4s$ ,  $4p$ ,  $4d$ , and  $4f$  shells are highlighted. The largest contribution comes from the ionization of the  $4d$  electron. As it is shown above, the EA channel for the excitations from the  $4d$  shell has also the largest impact compared to the  $4s$  and  $4p$  contributions (Fig. 4). For the DI process, the influence of the  $4s$  shell is very small. To ensure



our data can be easily utilized in modeling studies, we present the total ionization cross sections Table II.

It can be seen that the EA process increases the total cross section at the peak nearly by 40 % (Fig. 6). This contribution would be about two times smaller if the excitations to the higher shells ( $n \geq 9$ ) were not considered. The EA channels which include only the excitations with  $n \leq 8$  and  $l \leq 3$  provide for the EA process approximately 10% of the total cross section at the peak.

The ionization cross sections determined for the metastable  $[\text{Kr}]4d^{10}5s$  configuration are approximately by 60 % higher for the EA process compared to the ground configuration when the radiative damping is included for these configurations. The contribution of the indirect process from the high- $nl$  shells to the total cross sections increases by a factor of two. The DI from the  $5s$  shell is about two times higher for the metastable configuration compared to the ionization from the  $4f$  shell of the ground configuration.

#### IV. CONCLUSIONS

The contribution of the excitations to high- $nl$  shells has been studied for the electron-impact excitation-autoionization process. Calculations for the  $\text{W}^{27+}$  ion illustrate that the excitations to the high- $nl$  shells ( $9 \leq n \leq 40$ ) increase the cross section values by a factor of two for the indirect part of the ionization process. The largest contribution to the indirect part comes from the excitations to  $l = 4$  orbital. Surprisingly, large contribution also arises from the excitations to  $l = 5$  orbital. The EA cross sections for excitations from the  $4d$  shell to the shells with  $n \leq 8$  is approximately two times smaller compared to the excitations from the  $4p$  shell. On the other hand, situation drastically changes for the excitations to the higher shells with  $9 \leq n \leq 40$  where the excitations from the  $4d$  shell dominate. In this case,

the EA cross sections for the excitations from the  $4d$  shell are nearly three times higher. The current calculations for the  $W^{27+}$  ion show that the radiative damping has crucial effect on the cross sections of the indirect process. The cross section values decrease by two times for the LLDW results. However, the influence of the radiative damping to the subconfiguration-average cross sections is approximately 30 % smaller compared to the influence in the level-to-level calculations.

Current results demonstrate that the contribution of the EA channels originating from the excitations to the high- $nl$  shells has to be estimated in the analysis of the electron-impact ionization process for the highly charged ions. Good agreement with experiment for the low-charge states does not ensure that the same list of the investigated shells for the EA process is enough when the higher-charge states are considered. In order to estimate the contribution from the high- $nl$  shells, the convergence of the cross sections of the EA process must be checked.

#### ACKNOWLEDGEMENT

This research was funded by European Social Fund under the Global Grant Measure (No.: VP1-3.1-ŠMM-07-K-02-015). Part of computations was performed on resources at the High Performance Computing Center HPC Saulėtekis in Vilnius University Faculty of Physics.

- 
- [1] A. Kallenbach, R. Neu, R. Dux, H.-U. Fahrbach, J. Fuchs, L. Giannone, O. Gruber, A. Herrmann, P. Lang, B. Lipschultz, C. F. Maggi, J. Neuhauser, V. Philipps, T. Putterich, V. Rohde, J. Roth, G. Sergienko, A. Sips, and ASDEX Upgrade Team, Plasma Phys. Control. Fusion **47**, B207 (2005).

- [2] M. S. Pindzola, F. Robicheaux, S. D. Loch, J. C. Berengut, T. Topcu, J. Colgan, M. Foster, D. C. Griffin, C. P. Ballance, D. R. Schultz, T. Minami, N. R. Badnell, M. C. Witthoef, D. R. Plante, D. M. Mitnik, J. A. Ludlow, and U. Kleiman, *J. Phys. B* **40**, R39 (2007).
- [3] J. Colgan and M. Pindzola, *Eur. Phys. J. D* **66**, 284 (2012).
- [4] V. Jonauskas, A. Pranciševičius, Š. Masys and A. Kynienė, *Phys. Rev. A* **89**, 052714 (2014).
- [5] R. G. Montague and M. F. A. Harrison, *J. Phys. B* **17**, 2707 (1984).
- [6] M. Stenke, K. Aichele, D. Harthiramani, G. Hofmann, M. Steidl, R. Volpel, and E. Salzborn, *J. Phys. B* **28**, 2711 (1995).
- [7] M. Stenke, K. Aichele, D. Hathiramani, G. Hofmann, M. Steidl, R. Volpel, V. Shevelko, H. Tawara, and E. Salzborn, *J. Phys. B* **28**, 4853 (1995).
- [8] M. S. Pindzola and D. C. Griffin, *Phys. Rev. A* **56**, 1654 (1997).
- [9] S. D. Loch, J. A. Ludlow, M. S. Pindzola, A. D. Whiteford, and D. C. Griffin, *Phys. Rev. A* **72**, 052716 (2005).
- [10] V. Jonauskas, S. Kučas, and R. Karazija, *Lith. J. Phys.* **49**, 415 (2009).
- [11] J. Rausch, A. Becker, K. Spruck, J. Hellhund, A. J. Borovik, K. Huber, S. Schippers, and A. Mller, *J. Phys. B* **44**, 165202 (2011).
- [12] D. H. Zhang and D. H. Kwon, *J. Phys. B* **47**, 075202 (2014).
- [13] M. F. Gu, *Can. J. Phys.* **86**, 675 (2008).
- [14] A. E. Kramida and J. Reader, *At. Data Nucl. Data Tables* **92**, 457 (2006).

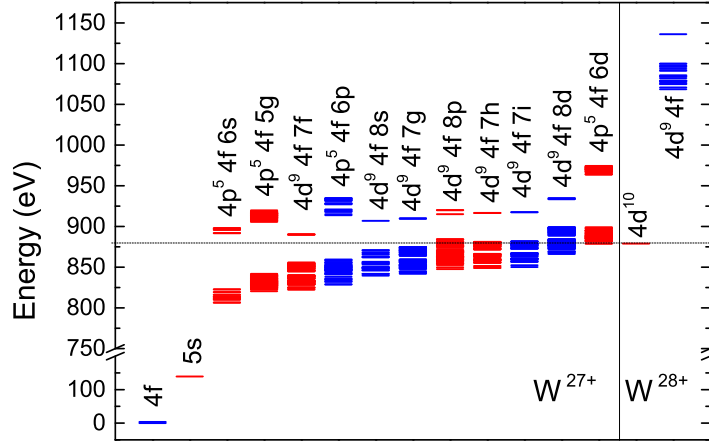


FIG. 1. (Color online) Energy levels of two lowest configurations and configurations which straddle the ionization threshold for the  $W^{27+}$  ion. Red color – even configurations, blue color – odd configurations.

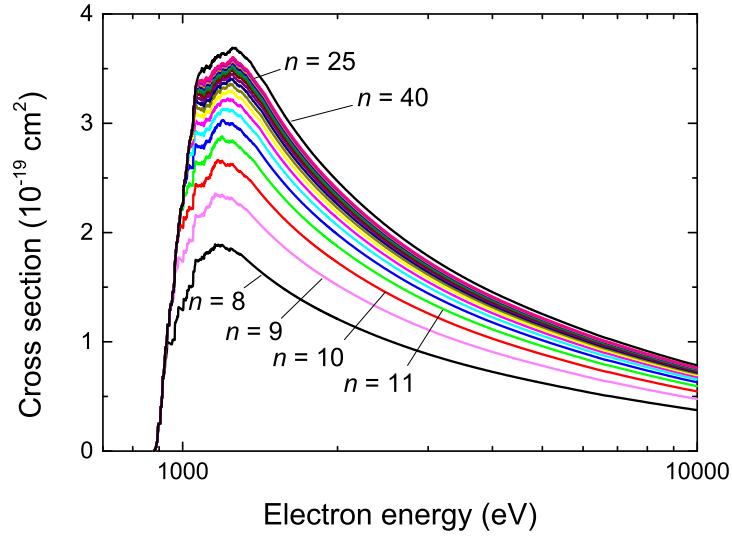


FIG. 2. (Color online) EA channels to the high- $nl$  shells for the  $W^{27+}$  ion. SCADW calculations.

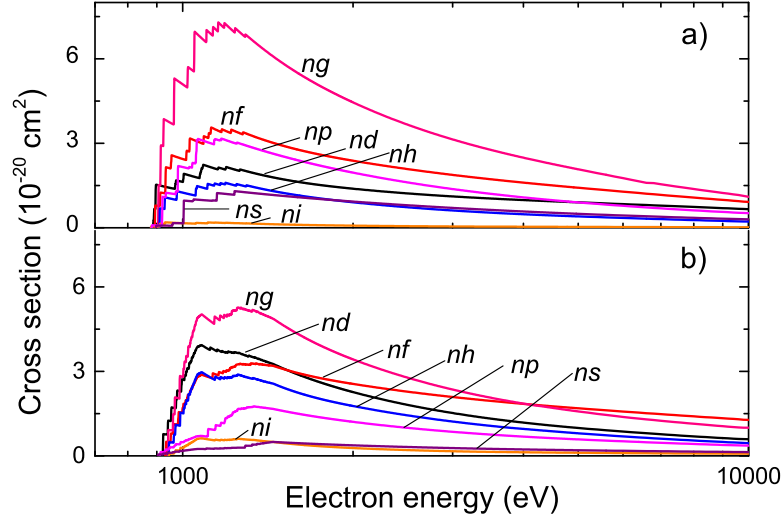


FIG. 3. (Color online) EA cross sections corresponding to excitations to various orbitals: a)  $n \leq 8$ , b)  $9 \leq n \leq 40$ . SCADW calculations.

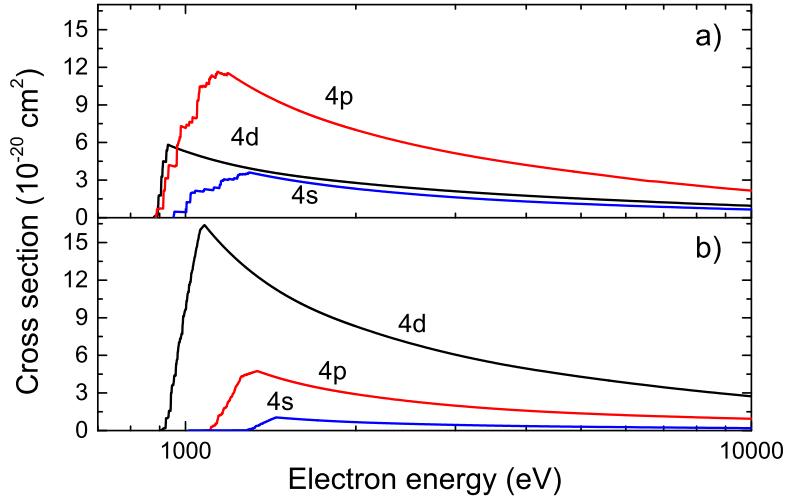


FIG. 4. (Color online) EA cross sections corresponding to excitations from the  $4s$ ,  $4p$ , and  $4d$  shells: a)  $n \leq 8$ , b)  $9 \leq n \leq 40$ . SCADW calculations.

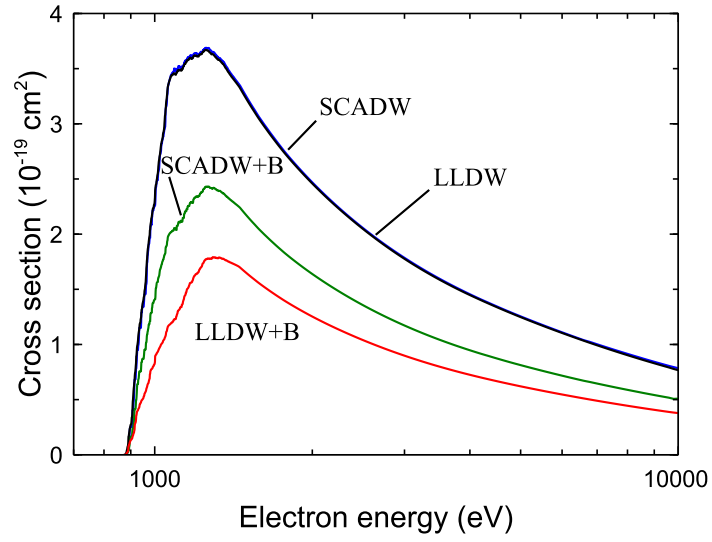


FIG. 5. (Color online) LLDW and SCADW cross sections for the EA process without (LLDW: black, SCADW: blue) and with (LLDW+B: red, SCADW+B: green) radiative damping.

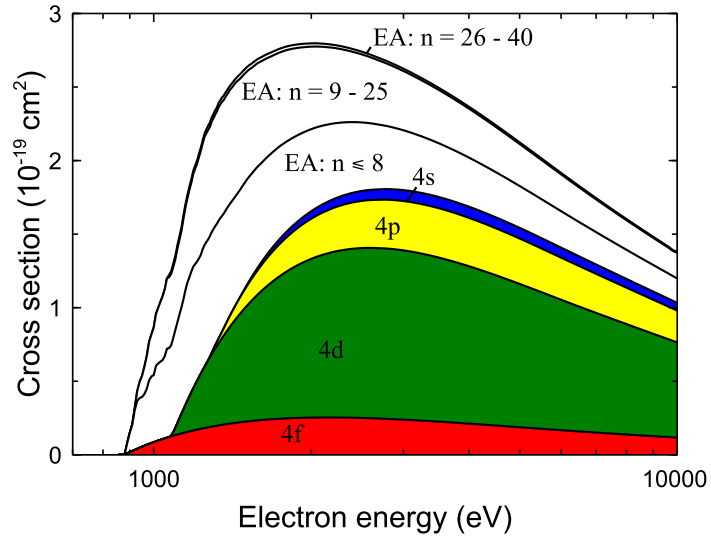


FIG. 6. (Color online) Total LLDW ionization cross section for the  $W^{27+}$  ion. The contributions of DI from different shells are highlighted by different colors. EA contributions from the excitations to various shells are presented.

TABLE I. Theoretical lowest energy levels (in eV) of the configurations of  $W^{27+}$ ,  $W^{28+}$ , and  $W^{29+}$  ions.

Ion	Level	Energy
$W^{27+}$	$4f(5/2)$	0.
	$4f(7/2)$	3.70
	$5s(1/2)$	139.33
$W^{28+}$	$4d^{10}(0)$	878.89
	$4d_{5/2}^5 4f_{5/2}(0)$	1068.57
	$4p_{3/2}^3 4f_{5/2}(1)$	1266.25
	$4s 4f_{5/2}(2)$	1458.42
	$3d_{5/2}^5 4f_{5/2}(0)$	2743.71
$W^{29+}$	$4d_{5/2}^5(5/2)$	2006.64
	$4d_{3/2}^3(3/2)$	2023.13



TABLE II: DI and EA cross sections (in  $10^{-20}$  cm<sup>2</sup>) for the  $W^{27+}$  ion. DI corresponds to the ionization from the  $4s$ ,  $4p$ ,  $4d$ , and  $4f$  shells. The EA contributions from the  $n \leq 8$ ,  $n \leq 25$ , and  $n \leq 40$  are also presented.

Energy (eV)	DI				EA			Total
	$4s$	$4p$	$4d$	$4f$	$n \leq 8$	$n \leq 25$	$n \leq 40$	
880				0.010	0.018	0.018	0.018	0.028
890				0.096	0.701	0.701	0.701	0.797
900				0.179	1.313	1.316	1.316	1.495
930				0.409	3.256	3.920	3.920	4.329
940				0.481	3.372	4.478	4.478	4.959
950				0.549	3.382	4.817	4.817	5.366
960				0.615	3.515	5.382	5.382	5.997
990				0.800	4.529	7.392	7.392	8.192
1000				0.857	4.558	7.798	7.798	8.655
1010				0.913	5.140	8.667	8.667	9.580
1020				0.966	5.240	9.024	9.024	9.990
1050				1.116	5.591	10.146	10.146	11.262
1060				1.163	6.059	10.821	10.853	12.016
1070			0.001	1.208	6.040	10.862	11.006	12.215
1080			0.063	1.252	6.143	10.988	11.181	12.496
1090			0.251	1.294	6.410	11.224	11.463	13.009
1120			1.074	1.413	7.063	12.143	12.378	14.865
1130			1.346	1.450	7.236	12.439	12.677	15.474
1140			1.614	1.486	7.490	12.964	13.199	16.300
1160			2.136	1.555	8.036	13.756	13.986	17.677
1180			2.630	1.619	8.207	14.256	14.482	18.732
1200			3.096	1.680	8.184	14.668	14.890	19.666
1240			3.956	1.791	8.230	15.400	15.615	21.361
1280		0.051	4.727	1.888	8.186	15.619	15.911	22.577
1340		0.374	5.742	2.014	7.954	15.677	15.964	24.094
1410		0.817	6.744	2.134	7.536	15.262	15.543	25.239
1460	0.002	1.107	7.358	2.206	7.307	14.874	15.183	25.855
1500	0.064	1.311	7.797	2.256	7.182	14.558	14.858	26.286
1650	0.252	1.918	9.107	2.394	6.589	13.305	13.578	27.249
1880	0.441	2.518	10.374	2.503	5.874	11.820	12.059	27.895
2000	0.510	2.731	10.794	2.527	5.576	11.185	11.409	27.970
2080	0.548	2.845	11.007	2.535	5.399	10.810	11.026	27.961
2300	0.627	3.077	11.389	2.529	4.971	9.927	10.124	27.746
2400	0.654	3.151	11.487	2.518	4.805	9.585	9.775	27.585
2700	0.710	3.294	11.579	2.463	4.391	8.742	8.914	26.959

Continued on next page

TABLE II: (continued)

Energy (eV)	DI				EA			Total
	$4s$	$4p$	$4d$	$4f$	$n \leq 8$	$n \leq 25$	$n \leq 40$	
3000	0.742	3.355	11.505	2.389	4.068	8.094	8.253	26.244
3500	0.762	3.355	11.158	2.253	3.655	7.284	7.426	24.955
3700	0.763	3.334	10.982	2.198	3.520	7.020	7.157	24.435
4100	0.758	3.271	10.605	2.091	3.280	6.556	6.684	23.410
4600	0.742	3.171	10.122	1.966	3.023	6.052	6.171	22.173
6000	0.681	2.861	8.870	1.672	2.479	4.981	5.080	19.163
7000	0.637	2.656	8.133	1.511	2.199	4.426	4.513	17.449
8000	0.595	2.474	7.506	1.379	1.981	3.993	4.072	16.026
9000	0.558	2.311	6.959	1.266	1.808	3.653	3.725	14.819
10000	0.526	2.169	6.481	1.171	1.660	3.401	3.470	13.381

Continued on next page